ASEAN Journal of Chemical Engineering 2024, Vol. 24, No. 2, 141 – 155

Statistical Analysis of Activation Factors for Coffee Husk Derived Activated Carbon on Chromium (VI) Adsorption and Carbon Yield

***Ngo Thi Thuan*[*,1,2]**
***Nguyen Minh Ngoc*[2,3]**
***Ly The Nghia*[2,3]**
***Tran Thi Hong Thu*[2,3]**
***Nguyen Duy Dat*[4]**
***Chanatip Samart*[5]**
[1]*School of Chemical and Environmental Engineering, International University, Quarter 6, Linh Trung Ward, Thu Duc City, Ho Chi Minh City 700000, Vietnam.*
[2]*Vietnam National University, Linh Trung Ward, Thu Duc District, Ho Chi Minh City 700000.*
[3]*Faculty of Environment, University of Science, Ward 4, District 5, Ho Chi Minh City 700000, Vietnam.*
[4]*Faculty of Chemical and Food Technology, Ho Chi Minh City University of Technology and Education, Ho Chi Minh 700000, Viet Nam.*
[5]*Department of Chemistry, Faculty of Science and Technology, Thammasat University, Pathumthani, 12120, Thailand*
*e-mail: ntthuan@hcmiu.edu.vn

Submitted 1 February 2024 *Revised* 18 April 2024 *Accepted* 16 June 2024

Abstract. Coffee husk waste, an abundant waste material in Vietnam, has been utilized to produce activated carbon. However, the single and interactional effects of activation factors for pyrolysis of coffee husk waste have not been studied well. This research proposed a fully statistical strategy including Box-Behnken experimental design, analysis of variance, regression diagnostics, influence degree, optimization and test of good-fitness, analysis of activated carbon's surface, and aimed to explore activation factors of impregnation ratio (IR) between H_3PO_4 and the biomass, activation temperature (AT) and time on Cr(VI) adsorption and carbon yield. The antagonistic effects of first-order AT and second-order IR contributed 75.91% of total influence factors and had the greatest impact on carbon yield. In contrast, the second-order AT, IR and the first-order IR, AT, their interaction accounting for 94.77%, had a statistically significant influence on Cr(VI) adsorption capacity. The optimal values of 35% IR, 540°C and 72 minutes could give 72.67±4.13% carbon yield, 104.13±7.64 mg Cr(VI) g^{-1}, and a specific surface area of 1896 m^2 g^{-1} due to an abundance of micropores, mesopores and hydroxyl, carbonyl and carboxylic groups on the biochar's surface. These findings suggest that the coffee husk waste-derived activated carbon may be a promising adsorbent for Cr(VI) and other small to medium-sized compounds from water, and the second-order polynomial regression model can be used to interpret the pyrolysis conditions to reduce preparation time and overall cost.

Keywords: Activated Carbon, Activation Factor, Chromium Adsorption, Coffee Husk, Response Surface Methodology

DOI: 10.22146/ajche.12034

INTRODUCTION

Activated carbon (AC) is a typical adsorbent used to remove numerous contaminants from wastewater, and its precursors are usually high-cost coals. AC demand has increased annually in the last decade, predicted up to 8.20% by 2028 due to industrial and agricultural activity growth (www.expertmarketresearch.com). In recent years, there have been various low-cost adsorbents that are prepared from any materials with simple processing, abundant in nature or waste material from industry and agriculture such as date palm seed (Reddy *et al.*, 2012), rice husk (Salleh *et al.*, 2014), mango peel waste (Ahmad and Alrozi, 2010), and coffee husk (Hernández Rodiguez *et al.*, 2018). Vietnam is the second largest coffee producer in the world; and 1 kg of dried coffee beans release an equivalent amount of coffee husk (France *et al.*, 2009; ICO, 2019). However, most coffee husks in Vietnam are used to make fertilizers or improperly burnt, releasing potentially hazardous contaminants into the environment due to highly bioactive components such as caffeine, trigonelline, and phenolics present in coffee husks. In addition, proximate components were widely published with variability of lipids (0.3–3%), protein (7–17%), ash (3–7%) and carbohydrates (16–85%) or cellulose (14.7–46.1%), hemicellulose (10.2–29.7%) and lignin (10.1–34.2%) (Cangussu *et al.*, 2021) which are appropriate to be a precursor for activated carbon. In this research, coffee husk, a cheap and plentiful raw material in Vietnam, was used to make activated carbon (AC), and converting coffee husk into AC to remediate pollutants is one of sustainable ways to add value to the circular economy in some post-harvest companies. AC-based coffee husk has been applied to investigate the adsorption processes such as Ni(II) ions (Hernández Rodiguez *et al.*, 2018), Pb(II) and Cd(II) ions (Quyen *et al.*, 2021), methylene blue (Oliveira *et al.*, 2008). Fundamentally, AC can be activated with either physical or chemical activation, and chemical activation with chemicals utilization under free-oxygen conditions increases specific surface area with well-controlled porosity, operates at lower temperatures, and produces more yields than physical activation (Wang *et al.*, 2014; Nayak *et al.*, 2017; Husain *et al.*, 2023). For example, a 4-fold increase of the $ZnCl_2$ amount to activate AC originating from coffee husk may triple the specific surface area (Gonçalves *et al.*, 2013). The presence of NaOH during pyrolysis could triple the specific surface area of coffee husk-derived AC (Quyen *et al.*, 2021). Acid phosphorous (H_3PO_4) is a widely used activating agent due to its free corrosion, low cost, and minimal air pollutant emission during pyrolysis (Nayak *et al.*, 2017; Wang *et al.*, 2014). Keeping other factors constant and changing one variable is a traditional way to explore conditions of ACs produced from coffee husk (Hernández Rodiguez *et al.*, 2018; Quyen *et al.*, 2021; Thuy Luong Thi *et al.*, 2021; Ngueabouo *et al.*, 2022), spent ground coffee (Jutakridsada *et al.*, 2016), coffee residue (Lamine *et al.*, 2014), but it takes time and can not evaluate interaction of crucial variables. Different cellulose, hemicellulose and lignin chemical components are also responsible for carbon yield production and adsorption. respectively (Lamine *et al.*, 2014; Jutakridsada *et al.*, 2016). Response Surface Methodology (RSM) is a useful statistical tool for optimizing production and analyzing its parameter impacts. RSM was applied to clarify the variation of parameters in the production of AC from mangosteen peel (Ahmad and Alrozi, 2010), Teff husk (Adane *et al.*, 2020), coconut

shell (Hu and Srinivasan, 1999), durian fruit peels (Le and Le, 2013), prosopis africana seed (Rahim and Garba, 2016). However, optimization of AC production from coffee husk waste (CHAC) and evaluation of either single or interaction impact and their contributions on two outcome responses, CHAC yield, and Cr(VI) adsorption capacity, has not been reported. Additionally, the CHAC characterizations at the optimal conditions have not yet been compared to others. In this work, Box Behnken Design (BBD), a subset of response surface methodology, was used to create experiment numbers and design with three important CHAC pyrolysis variables: impregnation ratio (IR), activation temperature (AT), and time. A regression between the outcome responses and variables was described as a mathematical model to evaluate statistically the single and interaction effects of production parameters and improve AC preparation from the coffee husk. In addition, CHAC characteristics at optimal level were identified and compared to other conditions by Brunauer-Emmett-Teller specific surface area and Fourier transform infrared spectroscopy to illustrate these effects on CHAC production.

MATERIALS AND METHODS

Materials

Coffee husk (CH) was collected at a local coffee manufacturer in Lam Dong Province, Vietnam, and is made of Robusta coffee. Chemicals of Potassium Dichromate ($K_2Cr_2O_7$) and 1,5-diphenylcarbazide with analytical grade (ACS, Reag. Ph Eur) were bought from Merck, Germany. Other chemicals, including phosphorous acid (H_3PO_4, 85%), acetone (CH_3COCH_3, 99.5%), sodium hydroxide (NaOH, 98%), hydrochloric acid (HCl, 36%) with lab grade, were purchased from Xilong Scientific Co. Ltd, China.

Preparation of CHAC Adsorbent

CH collected from the market was rinsed to discard some dirt and foreign items, and then naturally dried under the sun for several days. Finally, it was ground vigorously with a crusher and sieved to size 6 mm, which looks like homogeneous powder, so-called powder coffee husk (PH). Fiber characterizations of coffee husk were determined by thermalgravimetric analysis. The results of these components in the coffee husk are summarized in Table 1.

Table 1. Fiber characterizations of coffee husk

Parameters	Value (%)
Cellulose	40.30±8.00
Hemicellulose	20.25±5.60
Lignin	30.56±5.36

Carbonization and chemical activation are the two-step preparation for coffee husk-derived activated carbon, which has been described in some previous studies (Rodriguez *et al.*, 2011; Ngueabouo *et al.*, 2022; Husain *et al.*, 2023; Yi *et al.*, 2023). Firstly, 10 grams of PH was carbonized at 200°C for 1 h under constant N_2 flow with 100 cm^3/min@STP. Secondly, the carbonized PH sample was impregnated in a concentrated H_3PO_4 with a ratio ranging from 10 to 40 % (% of w/w, defined as the mass of phosphorus acid determined from its density and dried mass of coffee husk) for 5 hr, well-mixed to have a homogeneous slurry and dried at 105°C for 12 hr and placed in a desiccator. These dried samples were placed in a horizontal quartz reactor, fastened with two quartz wool plugs, and heated at a flow rate of 10°C min^{-1} to the desired activation temperatures ranging from 200 to 600°C

under an N_2 environment, kept at the desired temperatures for different activation times from 10 to 120 min, then cooled down under N_2 flow. Finally, the product was neutralized by sequentially soaking with NaOH 0.1N, hot water, and cold distilled water, respectively, and dried at 110°C for 5 hrs. Finally, the sample was crushed and sieved to collect a particle diameter of 2 mm and kept in an airtight bag for further experiments.

The carbon yield denoted as Y_1 is regarded to be an indicator of the carbonization process and evaluates the total cost of preparation conditions. CHAC yield can be calculated in the Eq. (1):

$$Y_1(\%) = \frac{W_2}{W_1} \times 100 \quad (1)$$

Where W_1: mass of coffee husk powder (g); W_2: mass of CHAC product (g)

Adsorption Experiments

Batch adsorption experiments of Cr(VI) on CHAC have been widely published elsewhere (Ahmad *et al.*, 2009; Le and Le, 2013; Mohamad Nor *et al.*, 2013). Basically, the experiments were conducted under 50 ppm Cr(VI) solution with a CHAC dosage of 0.01g, adsorption time of 30 minutes for equilibrium state, and initial pH2 with constant stirring speed at 200 rpm. After adsorption, the water sample was filtrated with 0.45 μm (Whatman filter paper) and complexed with 1,5-diphenylcarbazide, then the metal solution was measured with the absorbance at wavelength of 541 nm with UV-VIS spectrophotometer (Hach DR6000). Each experiment was triplicated and Cr(VI) adsorption capacity on CHAC described as Y_2 was calculated by Eq. (2).

$$\boldsymbol{Y_2 = q_e\left(\frac{mg}{g}\right) = \frac{(C_o - C_e)\times V}{m}} \quad (2)$$

Where C_o: initial Cr(VI) concentration (mg L^{-1}); C_e: Cr(VI) concentration at equilibrium time (mg L^{-1}); V: sample volume (L); m: dosage of CHAC (g).

Experimental Design and Statistical Analysis

In this research, Box-Behnken design (BBD) was employed to estimate single and interactional effects of AC production variables, including IR (X_1), time (X_2), and AT (X_3). Experimental number (N) required for development of BBD is from Eq. (3).

$$\begin{aligned} N &= 2k(k-1) + C_o \\ &= 2 \times 3 \times (3-1) + 5 \\ &= 17 \end{aligned} \quad (3)$$

Where k is the number of variables and C_o is a number of central points. Three variables were studied, including IR (%), time (min), and AT (°C).

A second-order polynomial regression model equation was used to express the outcome response (Y) regarding CHAC yield (Y_1) and Cr(VI) adsorption capacity (Y_2) as a function of the AC pyrolysis variables (X), which are coded and expressed by Eq. (4).

$$Y = \beta_0 + \sum_{i=1}^{k} \beta_i X_i + \sum_{i=1}^{k} \beta_{ii} X_i^2 + \sum_{i=1}^{k-1} \sum_{j=2}^{k} \beta_{ij} X_i X_j + \varepsilon \quad (4)$$

Where i = 1 →3, j = 1→ 3 and i≠j, β_0, β_i, β_{ii}, β_{ij} are intercepted constant, regression coefficients of linear, quadratic, and interaction effects, respectively. ε is residual, described as the difference between measured and predicted results. The ranges and levels of the independent variables are given in Table 2. The max, min and center values were coded as +1, 1, and 0, respectively. Variables of IR, time and AT were coded as X_1, X_2, X_3 for various effects of linear (X_1, X_2, X_3), pure quadratic (X_1^2, X_2^2, X_3^2) and

two variables' interactions (X_1X_2, X_1X_3, X_2X_3). Positive and negative signs of each term reflect synergistic and antagonistic influences on the responses, respectively.

Table 2. Experimental levels and ranges in Box-Behnken experimental design

Symbol	Factors	Variable level and range		
		-1	0	+1
X_1	IR (%)	10	25	40
X_2	Time (min)	10	65	120
X_3	AT (°C)	200	400	600

Analysis of Variation (ANOVA) and regression analysis was applied to evaluate the statistical significance of regression coefficients, model comparisons, and model diagnostics. The regression model with the best parameters was validated by confirmatory experiments using Eq. 4. ANOVA was conducted to determine model fitness and statistical significance of linear (FO), pure quadratic effects (PQ), and two variables' interactions (TWI). These terms are statistically significant when the Fisher test with Pr (>F) value is < 0.05 and variation sources are greater with lower Pr(>f) value and larger F-values. The estimated coefficient is statistically significant when the Pr (>|t|) value is less than 0.05.

Regression Diagnostics

Regression diagnostics were carried out to examine the satisfaction of the statistical assumptions for regression. Diagnostic tools include plots of Residuals vs. Fit, Scale-location, residuals vs. Leverage, and Normal Q-Q incorporated with Shapiro-Wilk and Durbin-Watson tests to assess heteroscedasticity assumptions, normality, and influenced outliers, respectively. In addition, predicted values of CHAC yield and Cr(VI) adsorption capacity were calculated by substituting the coded values into Eq. 5 & 6, then plotted with experimental results of the Y_1 and Y_2 responses. All these statistical analyses were undertaken with the support of R Studio software (version 3.6.1) with package "RSM" (Lenth, 2009) and *gg-plot*.

INFLUENCE DEGREES

The influence degree of each factor was calculated by each statistically significant coefficient (β_i) to have a contribution (%) on the response via Pareto analysis and described in the following Eq. (5) (Xu *et al.*, 2013).

$$ID(\%) = \frac{\beta_i^2}{\sum \beta_i^2} \times 100 \quad (5)$$

Characterizations of Optimal CHAC Adsorbent

Specific surface area (S_{BET}), pore size distribution, and total volumes of CHAC were determined from the N_2 sorption isotherm data with the BET (Brunauer, Emmett, and Teller) method (Quatachrome NOVA 1000E). Functional groups of CHAC adsorbents were examined with Fourier transform infrared (FTIR) spectroscopy (NIR MIR Perkin Elmer) with KBr pellet and scanned within a wavelength range of 400–4000 cm^{-1}.

RESULTS AND DISCUSSION

Development of Regression Models

The corresponding 17 experiments of 3 factors with 2 levels were assigned by Box-Behnken design (BBD), and their results are shown in Table 3.

$$Y_1 = 77.37 + 8.27X_1 - 2.08X_2 - 12.86X_3 + 0.78X_1X_2 + 1.41X_1X_3 - 0.645X_2X_3 - 12.22X_1^2 - 0.93X_2^2 + 4.82X_3^2 \quad (6)$$

$$Y_2 = 94.80 + 20.77X_1 + 5.17X_2 + 26.22X_3 - 0.39X_1X_2 + 17.01X_1X_3 - 2.61X_2X_3 - 27.11X_1^2 - 11.43X_2^2 - 28.94X_3^2 \quad (7)$$

Analysis of Variance (ANOVA)

Table 4 indicated that the linear (FO) and pure quadratic effects (PQ) were statistically significant on both response Y_1 (CHAC yield) and Y_2 (Cr(VI) adsorption capacity) with Pr(>F) values less than 0.05 whereas two variable interactions were not statistically significant on both responses of Y_1 and Y_2 at significant level of 0.05 but statistically significant on Y_2 at that of 0.2. Effect of individual term in the Eq. (6) and (7) were further analyzed through the estimated coefficients, and their Pr(>|t|) values were summarized in Table 5. In the Table 5, the estimated coefficients with Pr(>|t|) values less than 0.05 for Y_1 response were 8.27, -2.08, -12.86, -12.22 and 4.83 of X_1, X_2, X_3, X_1^2 and X_3^2, respectively whereas those for Y_2 response were 20.77, 26.22, 17.01, -27.11 and -28.94 of X_1, X_3, X_1X_3, X_1^2 and X_3^2, respectively. These results implied that single effect of IR and AT contributed statistically and followed the linear and quadratic effect

Table 3. Experimental design

Batch no.	Coded values			Uncoded values			Responses	
	X_1	X_2	X_3	IR (%)	Time (min)	AT (°C)	Y_1(%)	Y_2(mg/g)
1	0	0	0	25	65	400	79.03	99.32
2	0	0	0	25	65	400	77.61	87.63
3	+1	0	+1	40	65	600	66.64	94.91
4	+1	0	-1	40	65	200	87.95	18.47
5	0	0	0	25	65	400	78.66	102.03
6	0	0	0	25	65	400	76.78	97.36
7	+1	-1	0	40	10	400	75.81	73.97
8	-1	-1	0	10	10	400	58.91	18.69
9	-1	+1	0	10	120	400	51.09	39.36
10	0	-1	-1	25	10	200	95.29	16.56
11	0	0	0	25	65	400	74.77	87.68
12	0	+1	-1	25	120	200	94.54	22.57
13	0	+1	+1	25	120	600	65.94	87.10
14	-1	0	-1	10	65	200	76.13	23.89
15	-1	0	+1	10	65	600	49.18	25.01
16	+1	+1	0	40	120	400	71.09	93.05
17	0	-1	+1	25	10	600	69.27	91.51

Table 4. ANOVA of CHAC yield (Y_1) and Cr(VI) adsorption capacity (Y_2)

Source	CHAC yield (Y1)				Cr(VI) adsorption capacity (Y2)			
	Df	Mean Sq	F	Pr (>F)	Df	Mean Sq	F	Pr (>F)
FO (X_1,X_2,X_3)	3	635.0	135.3	1.47×10^{-6} ***	3	3055	16.5	0.0015 **
TWI (tal,X_2X_3, X_1X_3)	3	4.01	0.854	0.507	3	395	2.13	0.1811
PQ (X_{12},X_{22},X_{32})	3	236.5	50.40	4.17×10^{-5} ***	3	2628	14.2	0.0023**
Residual	7	4.69			7	185.3		

Table 5. Estimated coefficients of response Y_1 and Y_2

Coefficients	*CHAC yield (Y_1)*		*Cr(VI) adsorption capacity (Y_2)*	
	Estimate	**Pr(>|t|)**	**Estimate**	**Pr(>|t|)**
β_0	77.37	1.27×10^{-11} ***	94.80	1.088e-06 ***
β_1	8.27	1.284×10^{-5} ***	20.77	0.0034962 **
β_2	-2.08	0.030084*	5.17	0.3184185
β_3	-12.86	6.501×10^{-7} ***	26.22	0.0009575 ***
β_{12}	0.78	0.4974	-0.39	0.9550567
β_{13}	1.41	0.2341	17.01	0.0410293 *
β_{23}	-0.645	0.5702	-2.61	0.7132490
β_{11}	-12.22	8.115×10^{-6} ***	-27.11	0.0046483 **
β_{22}	-0.93	0.407565	-11.43	0.1286537
β_{33}	4.82	0.002587**	-28.94	0.0033009 **

*Signif. codes: 0 '***' 0.001 '**' 0.01 '*' 0.05 '.' 0.1 ' ' 1*

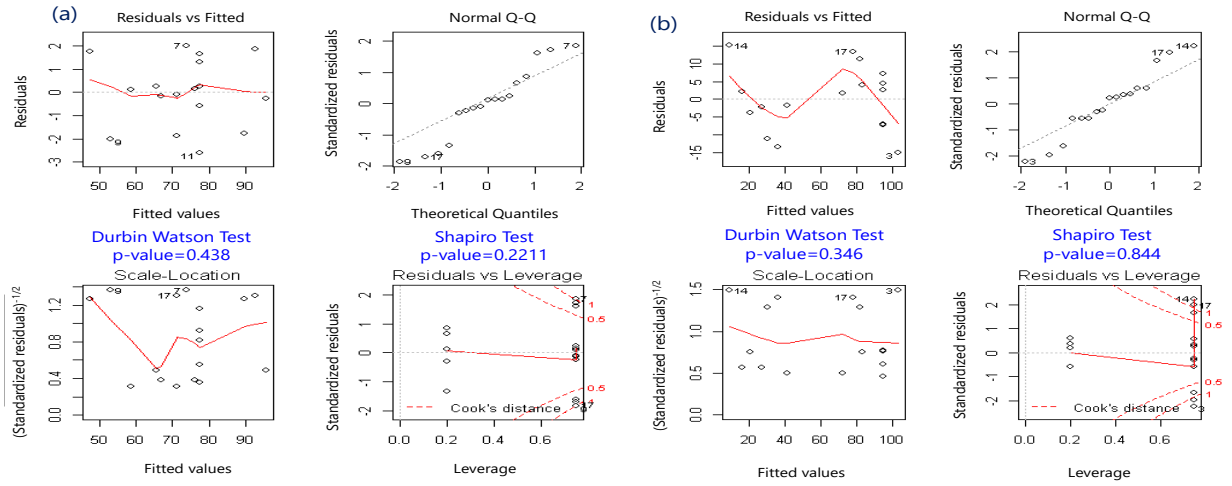

Fig. 1: Regression diagnostics of RMS model for CHAC yield (a) and Cr(VI) adsorption capacity (b)

on both CHAC yield and Cr(VI) adsorption capacity whereas time attributed linearly on CHAC yield. In addition, there is only interaction between IR and AT affecting statistically Cr(VI) adsorption capacity.

Regression Diagnosis

Fig. 1 a & b showed regression diagnosis for the empirical quadratic models of CHAC yield and Cr(VI) adsorption capacity, respectively, to examine model fitness appropriate with experimental data. In this study, the Residual vs. Fitted plot and Scale-location plot shown in Fig. 1a and 1b indicated the random distribution and gave the p-values of 0.438 and 0.344 in the Durbin Watson test. These p-values above 0.05 describe homogenous variances without other factors contributing to the studied responses.

The points in the Normal Q-Q plot distributed close to the diagonal line and p-values of 0.2211 and 0.8439 in the Shapiro-Wilk test are higher than 0.05, which demonstrates the satisfactory normality of those two models. The points in residuals vs. leverage plots approximately in a range of Cook's distance showed no influenced

outliers in these models. In addition, the Adj R^2 corresponded p-values for carbon yield and Cr(VI) adsorption capacity were 0.987 (p-value<<0.05) and 0.940 (p-value<<0.05) in Fig. 2 illustrating that the regression showed high fitness with the empirical quadratic Eq. (6) & (7) and these models can be applied to predict the responses within the investigated ranges.

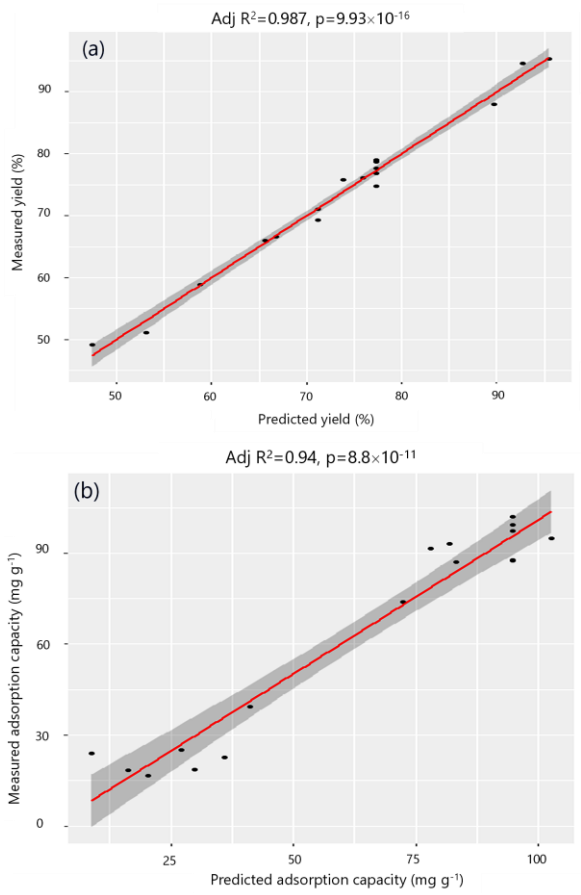

Fig. 2: Correlations between predicted values and measured results for CHAC yield (a) and Cr(VI) adsorption capacity (b)

Interpreting the Significant Influence of Pyrolysis Factors on The Responses

Influence of Pyrolysis Factors on CHAC Yield

In Eq. (6), negative signs of β_3(-12.86), β_2(-2.08), and β_{11}(-12.22) indicated antagonistic influences of first-order AT, time, and second-order IR, while positive signs of β_1 (+8.27) and β_{33} (+4.82) implied synergistic effects of first-order IR and second-order AT on the CHAC yield's response. Influence degrees of those coefficients were denoted in Fig. 3 in order as follows: first-order AT (39.91%)>second-order IR (36.00%)>first-order IR (16.50%)>second-order AT (5.61%)>first-order time (1.04%). The effects of the first-order AT and second-order IR are the most influences, accounting for approximately 75.91% of CHAC yield.

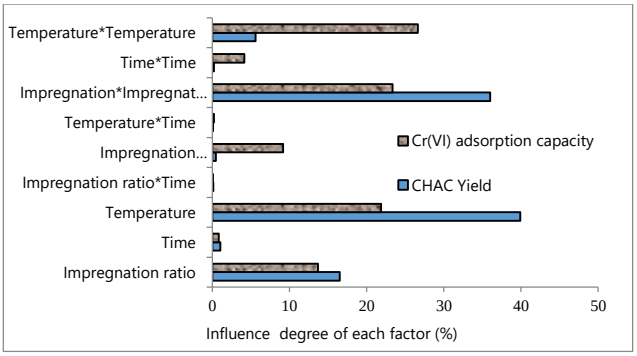

Fig. 3: Influence degrees of pyrolysis variables on the responses

Surface plots were also drawn based on the empirical quadratic Eq. (6) to visualize all these effects on response surfaces of CHAC yield shown in Fig. 4. The surface plots were prepared when two variables were changed at the constant third variable. Fig. 4a and 4b indicated that variations of IR and AT showed a significant effect, but time variation changed very little in terms of carbon yield. An increase in IR from 10 to 35% led to enhance the carbon yield. Then this yield decreased with IR above 35% (Fig. 4a). Enhancement of carbon yield obtained by H_3PO_4 amount ranging from 10 to 35% is possibly due to cross-linking formation of cellulose polymers presenting in the coffee husk that can keep the relatively low molecular weight species within the structure, but a breakdown of the cellulose polymer

chains occurred at high H_3PO_4 concentration due to high dehydration ability of the activated agent. Whereas the effect was observed to be negatively correlated with carbon yield and the most significant variable affecting the CHAC yield (Fig. 4b). This result is possibly explained by the loss of volatile compounds and then intensified dehydration and degradation of the lignocellulosic materials and aryl ether bond.

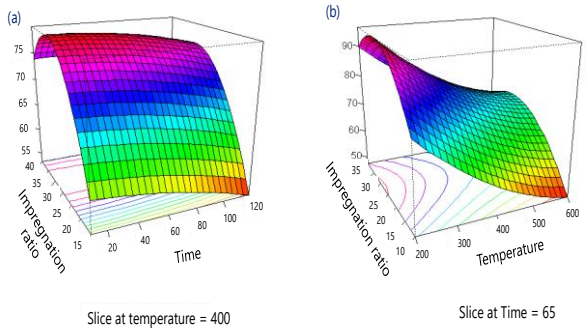

Fig. 4: 3D surface plots for influence of two variables on CHAC yield: (a) influence of IR and time at constant AT of 400°C, (b) influence of IR and AT at constant time of 65 min.

A similar trend for pyrolysis factors on activated carbon yield using H_3PO_4 from Raffia palm shells (Iwar *et al.*, 2021) was observed. But a slight difference in preparation conditions between mangosteen peel (Ahmad and Alrozi, 2010) and rattan sawdust (Ahmad *et al.*, 2009) were observed in which temperature imposed the greatest influence while the impregnation ratio was considerated to moderate degree, but time was not shown to effect on activated carbon yield for a case of KOH usage as an activation agent. However, the highest AC yield shown at the optimal region could not be achieved in the studied ranges of time, IR, and AT. The optimal condition for CHAC yield may be obtained at AT and time smaller than 200°C and 10 min, respectively, but they could not be recommended for the purpose of Cr(VI) adsorption. Further analysis of this statement will be evaluated in the following part.

Influence of Pyrolysis Factors on Cr(VI) Adsorption Capacity

In Eq. (7), positive signs of β_1 (20.77), β_3 (26.22), and β_{13} (17.01) implied the synergetic effects of first-order IR, AT, and their interaction on Cr(VI) adsorption capacity. In contrast, negative signs of β_{11} (-27.11) and β_{33}(-28.94) described the antagonistic influences of second-order IR and AT on Cr(VI) adsorption capacity. Influence degree (ID) of second-order AT, which accounted for 26.63% was the most influential factor, followed by second-order IR (23.36%), then first-order AT (21.86%), first-order IR (13.72%) and finally, the interaction term between IR and AT (9.20%). In addition, 3D surface plots shown in Fig. 5a indicated that an increase of IR from 10% to 40% can enhance Cr(VI) adsorption capacity from 19 mg g^{-1} to 99 mg g^{-1}, then reduce to 74 mg g^{-1}. At the same time, Fig. 5b showed that an increase of AT from 200–600°C can significantly improve Cr(VI) adsorption capacity from 30 mg g^{-1} to 102 mg g^{-1}, then decrease to 90 mg g^{-1}. No statistical significance of the time factor on Cr(VI) adsorption capacity was described in the estimated coefficient of β_2 (Table 5). Consequently, interaction terms between time or IR (Impregnation ratio) (Fig. 5a) or AT (Temperature) and time (Fig. 5b) could not be observed clearly. At the same time, combination of AT and IR had made a notable change of Cr(VI) adsorption capacity shown in Fig. 5c. These total influence degrees from synergetic and antagonistic influences contributed approximately 44.78 and 49.99%, respectively, which demonstrated the optimal value obtained in this investigated range.

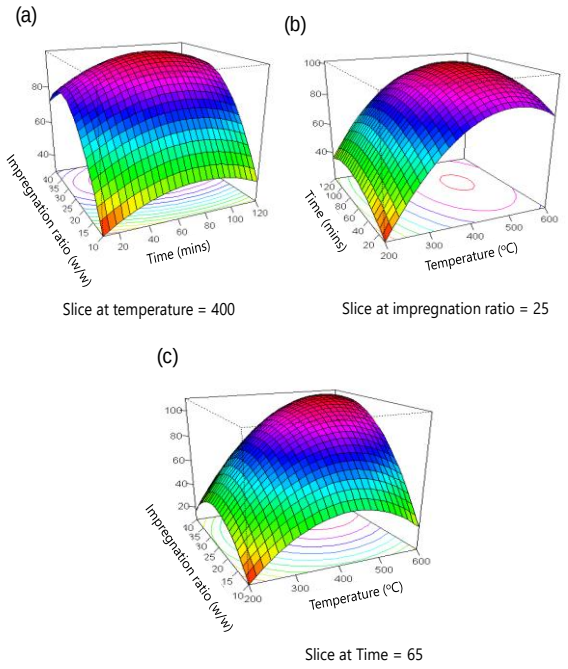

Fig. 5: Surface plots for influence of two factors on Cr(VI) adsorption capacity: (a) Influence of IR and time at constant AT of 400°C; (b) Influence of time and AT at constant IR of 25%; (c) Influence of IR and AT at constant time of 65 min.

Process Optimization

The optimal values of IR, time, and AT for Cr(VI) adsorption capacity were obtained by the response in Eq. (6) and then used to carry out the pyrolysis experiments to test agreement between the experimental values and those obtained from Eq. (6) and (7), finally shown in Table 6. It was indicated that the optimal conditions for CHAC production were 35%, 72 min, and 540°C. The Cr(VI) adsorption capacities at these optimal values obtained from experiments and statistical models were 104.13±7.64 mg g^{-1} and 111.69 mg g^{-1}, while the corresponding CHAC yield was 72.67±4.13% and 72.18%, respectively.

The p-values of experimental and predicted results for Cr(VI) adsorption capacity and CHAC yield were 0.103 and 0.467, respectively. These results indicated no statistical difference at the significant level of 0.05. Eq. (6) and (7) were successfully applied to quantify the maximum response of Cr(VI) adsorption capacity and the carbon yield within the examined ranges.

Table 6. Optimal values in the pyrolysis conditions for CHAC

IR (%)	Time (min)	AT (°C)	Cr(VI) adsorption capacity (mg g^{-1}) Prediction	Experiment	p-value
35	72	540	111.69	104.13±7.64	0.103
			CHAC yield (%)		
			72.18	72.67±4.13	0.467

Characterizations of CHAC Adsorbent

The nitrogen adsorption isotherms, pore size distributions, and functional groups of CHAC under optimal conditions (35% of IR, 540°C) denoted as IR35AT540 were investigated. These characterizations of IR35AT540 were also compared to those of CHAC prepared at the lowest level (10% of IR, 200°C) described as IR10AT200, and the highest one (40% of IR, 600°C), denoted as IR40AT600, to illustrate how IR and AT affect CHAC characterizations. Fig. 6a indicated the isotherms of the IR35AT540 and IR40AT600 following IUPAC type I and IV isotherms with hysteresis loops at high relative pressure, while IR10AT200 did not follow any typical isotherms. No typical isotherm of IR10T200 indicated that this IR10AT200 seemed not activated yet under the conditions of 10% IR and 200°C. As a result, the IR10AT200 gave the lowest BET surface area (0.135 m^2 g^{-1}). In comparison, both IR35AT540 and IR40AT600 exhibited a well-developed microporous-mesoporous structure that can achieve the high BET surface areas of 1896 m^2 g^{-1} and 1690 m^2 g^{-1}, respectively. In addition, the adsorbed volumes of IR35AT540 increased rapidly at low relative pressure (0–0.4), reaching a plateau quickly and exhibiting smaller hysteresis loops at the high relative pressure (0.4–1.0) than those of IR40AT600.

This result indicated that both micropore and mesoporous structures were present in CHAC under the optimal conditions. In addition, the pore size distribution of those 03 kinds of activated carbons as shown in Fig. 6b, exhibited a monomodal distribution in the range of micropore, which is typical for AC with two-step H_3PO_4 activation (Oginni *et al.*, 2019). The higher intense of micropore volume (0.056 cc $A^{o-1}g^{-1}$) at 17A° and a smaller range of pore sizes (10–55A°) presenting in IR35AT540 than those in IR40AT600 (0.046 cc $A^{o-1}g^{-1}$ at 18A°, 10–65A°) were observed. As a result, BET surface area and total pore volume of IR35AT540 and IR40AT600 were 1896 m^2g^{-1} vs. 1690 m^2g^{-1} and 0.842 cm^3g^{-1} vs. 0.967 cm^3g^{-1}. The higher BET surface area enhanced the number of adsorption sites, and a certain amount of microporous/mesoporous volumes allowed a fast mass transfer rate. This can help to explain the mechanism of the highest Cr(VI) adsorption capacity under these optimal conditions.

The functional groups on the surface of 03 CHAC types were determined by FTIR spectroscopy (Fig. 6c). The FTIR peaks of CHAC were attributable mainly to (i) –O–H stretching vibration of phenol, alcohols (3150–3500 cm^{-1}); (ii)–C≡C stretching vibration (2636–2644 cm^{-1}); (iii) –C=O groups incorporated into hydrogen bonds (1605–1628 cm^{-1}); (iv) –C–O bonds of alcohols and phenols (~1156 cm^{-1}); (vi) P–O–C groups (1030–1090 cm^{-1}). These peaks were typically found in activated carbon derived from biomass with an H_3PO_4 chemical agent (Daasch and Smith, 1951; Das and Mishra, 2017; Zhang *et al.*, 2018; Jawad *et al.*, 2020).

Intensity of –O–H groups at 3404 cm^{-1} decreased when temperature increased from 200 to 600°C and the three vibrations of –C=O, –C–O–P and –C–O and/or C–O–C increased as IR enhanced. However, the absorbent of IR35AT540 at the optimal conditions exhibited the highest intensity of –C=O, P–O–C, and –C–O and/or C-O-C stretching vibrations together –O–H groups. The results in IR35AT540 indicated an increase of these functional groups due to the interaction effect at the optimal conditions and possibly promoted interaction with basic species such as Cr(VI) ions in water.

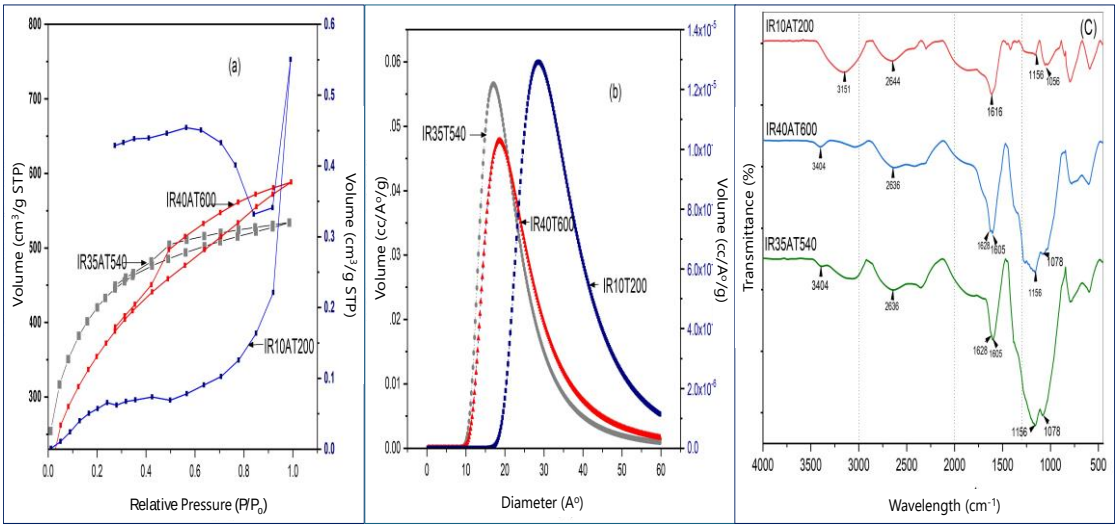

Fig. 6: Nitrogen adsorption isotherm (a); pore size distribution (b) and FTIR spectrum (c) of CHACs

Table 7. Characterizations of activated carbon derived from different types of biomass waste

Biomass waste	**Activation conditions** (% activated reagent/biomass; activation temperature; time)	**Adsorptive properties**				**Adsorption capacity (mg g^{-1})**	**Carbon yield (%)**	**Refs**
		Specific surface area (m^2 g^{-1})	Total Pore volume (cm^3 g^{-1})	Pore diameter (A°)	Functional groups			
Coffee husk	10% (Hydrothermal), 30 min, 800°C	383.0	0.151	5.8-8.4	Carboxyl, lactone and phenolic	57.14 (Ni^{2+})	---	Hernández Rodiguez *et al.*, 2018
Coffee husk	1M (NaOH), 500°C, 1 h	987.9	0.984	---	Oxygen-containing functional group	116.3 (Cd^{2+}) & 139.5 (Pb^{2+})	---	Quyen *et al.*, 2021
Raffia palm shell	76.91% (H_3PO_4), 103.83 min, 523.68°C	465.10	0.25	10-30	hydroxyl, carbonyl and carboxylic phosphorus oxides	---	79.44	Iwar *et al.*, 2021
Coffee husk	33% ($ZnCl_2$) 600°C, 2 h	1383	1.648	20-250	Acidic and basic groups	188.12 (RR 195)	---	Thuy Luong Thi *et al.*, 2021
Cassava sludge	20% ($ZnCl_2$), 500°C, 1 h	509.3	0.375	5-50	Hydroxyl, carboxyl, alkene, silicates, ketones	2.83 (Cr^{6+})	---	Guo *et al.*, 2021
Coffee husk	0.1M (H_3PO_4), 600°C, 120 min	560.65	---	---	pH_{pzc}=6.63	520.65 (Iodine)	67.236	Ngueabouo *et al.*, 2022
	0.1 M (KOH), 300°C, 120 min	520.55	---	---	pH_{pzc}=6.98	603.45 (Iodine)	59.054	
Coffee husk	**35% (H_3PO_4), 540°C, 72 min**	**1896**	**0.842**	**10-55**	**hydroxyl, carbonyl and carboxylic, phosphorus oxides**	**111.69 (Cr^{6+})**	**72.18**	**This study**

The specific surface area of 1896 m^2 g^{-1} at the optimal condition achieved in this study was higher than those obtained in the published research using the same precursor of the coffee husk (Hernández Rodiguez *et al.*, 2018; Quyen *et al.*, 2021; Thuy Luong Thi *et al.*, 2021; Ngueabouo *et al.*, 2022) (Table 7). The high specific surface area of CHAC produced at the optimal conditions is possibly attributed to the higher content of fiber components and volatile matter present in the coffee husk waste. The variety of these components depends on their geographic origin and production. In addition, the comparative results in Table 7 showed that H_3PO_4 acid is more efficient for micro and mesoporous development at low temperatures (<700°C) and gives higher carbon yield than base agents such as NaOH and $ZnCl_2$. This can be explained by the hydration and degradation abilities of phosphoric acid at the optimal temperature, described in the following chemical reactions. CO_2 gas was released during these processes to make activated carbon porosity (Neme *et al.*, 2022).

$H_{n+2}P_nO_{3n+1} \rightarrow P_4O_{10} + H_2O$

$P_4O_{10} + 2C \rightarrow P_4O_6 + 2CO_2$

A sufficient amount of H_3PO_4 and temperatures at 35% and 540°C, obtained with response surface methodology, can make pore sizes from 10 to 55 A°, typically micropores and a certain amount of mesopores, suitable toward Cr(VI) ion adsorption as well as other small to medium-sized compounds.

CONCLUSIONS

The influences of IR, AT and time on the CHAC yield and Cr(VI) adsorption capacity were examined using statistical tools in this study. The results showed that the first-order AT and second-order IR had the most significant influence on CHAC yield, while the second-order AT and IR imposed the greatest effect on Cr(VI) adsorption capacity. In addition, the interaction terms of AT and IR had a significant impact on the turning point of Cr(VI) adsorption capacity. The IR of 35%, 72 mins, and AT of 540°C were found as the optimal conditions of CHAC pyrolysis. The CHAC prepared at the optimal conditions had a specific surface area of 1896 m^2/g, almost microporous and mesoporous volumes, the pore diameter ranging from 10 to 55A°, a total pore volume of 0.842 cm^3/g and many oxygen-content functional groups include alkenyl, aromatic, alcohols, carboxylic acids, esters which are suitable for Cr(VI) adsorbent as well as other metal oxides or nanomaterials.

ACKNOWLEDGMENT

This research is funded by Vietnam National University HoChiMinh City (VNU-HCMC) under grant number B2022-28-07.

REFERENCES

Adane, T., Haile, D., Dessie, A., Abebe, Y., Dagne, H., 2020. "Response surface methodology as a statistical tool for optimization of removal of chromium (VI) from aqueous solution by Teff (*Eragrostis teff*) husk activated carbon." *Appl. Water Sci.* 10, 37.

Ahmad, A.A., Hameed, B.H., Ahmad, A.L., 2009. "Removal of disperse dye from aqueous solution using waste-derived activated carbon: Optimization study. *J. Hazard. Mater.* 170, 612–619."

Ahmad, M.A., Alrozi, R., 2010. "Optimization of preparation conditions for mangosteen peel-based activated carbons for the removal of Remazol Brilliant Blue R using response surface methodology." *Chem. Eng. J.* 165, 883–890.

Cangussu, L.B., Melo, J.C., Franca, A.S., Oliveira, L.S., 2021. "Chemical Characterization of coffee husks, a by-product of *Coffea arabica* production." *Foods 10*, 3125.

Daasch, L., Smith, D., 1951. "Infrared spectra of phosphorus compounds." *Anal. Chem.* 23, 853–868.

Das, S., Mishra, S., 2017. "Box-Behnken statistical design to optimize preparation of activated carbon from *Limonia acidissima* shell with desirability approach." *J. Environ. Chem. Eng.* 5, 588–600.

Gonçalves, M., Guerreiro, M.C., Oliveira, L.C.A., Solar, C., Nazarro, M., Sapag, K., 2013." Micro mesoporous activated carbon from coffee husk as biomass waste for environmental applications." *Waste Biomass Valorization 4*,395–400.

Guo, C., Ding, L., Jin, X., Zhang, H., Zhang, D., 2021. "Application of response surface

methodology to optimize chromium (VI) removal from aqueous solution by cassava sludge-based activated carbon." *J. Environ. Chem. Eng.* 9, 104785.

Hernández Rodiguez, M., Yperman, J., Carleer, R., Maggen, J., Dadi, D., Gryglewicz, G., Van der Bruggen, B., Falcón Hernández, J., Otero Calvis, A., 2018. "Adsorption of Ni(II) on spent coffee and coffee husk based activated carbon." *J. Environ. Chem. Eng.* 6, 1161–1170.

Hu, Z., Srinivasan, M.P., 1999. "Preparation of high-surface-area activated carbons from coconut shell." *Microporous Mesoporous Mater.* 27, 11–18.

Husain, C., Zawawi, N.,Hamzah, N. A., Mohd Rodhi, F., Veny, M. N., Ariyanti, H., & Mohidem, N. A., 2023. "Chemical properties and breakthrough adsorption study of activated carbon derived from carbon precursor from carbide industry." *ASEAN Journal of Chemical Engineering 23(2)*, 240-254.

Iwar, R.T., Ogedengbe, K., Katibi, K.K., Oshido, L.E., 2021. "Meso-microporous activated carbon derived from Raffia palm shells: optimization of synthesis conditions using response surface methodology." *Heliyon 7*, e07301.

ICO-International Coffee Organization. World Coffee Production, 2019. Available online: http://www.ico.org/pt/trade_statistics.asp (accessed on 1 December 2019).

Jawad, A.H., Bardhan, M., Islam, Md. Atikul, Islam, Md. Azharul, Syed-Hassan, S.S.A., Surip, S.N., ALOthman, Z.A., Khan, M.R., 2020." Insights into the modeling, characterization and adsorption performance of mesoporous activated carbon from corn cob residue via microwave-assisted H_3PO_4 activation." *Surf. Interfaces 21*, 100688.

Jutakridsada, P., Prajaksud, C., Kuboonya-Aruk, L., Theerakulpisut, S., Kamwilaisak, K., 2016. "Adsorption characteristics of activated carbon prepared from spent ground coffee." *Clean Technol. Environ. Policy* 18, 639–645.

France, A.S., Oliveria, L.S., 2009. "Coffee processing solid wastes:Current uses and future perspectives". In Agricultural Wastes; Ashworth, G.S., Azevedo, P., ed., Nova Science Publishers Inc.: Newyork, USA.

Lamine, S.M., Ridha, C., Mahfoud, H.-M., Mouad, C., Lotfi, B., Al-Dujaili, A.H., 2014. "Chemical activation of an activated carbon prepared from coffee residue." *Energy Procedia 50*, 393–400.

Le, P.T.K., Le, K.A., 2013."Optimisation of durian peel based activated carbon preparation conditions for dye removal." *Sci. Technol. Dev. J.* 16, 22–31.

Lenth, R.V., 2009. "Response-surface methods in *R*, using RSM." *J. Stat. Softw. 32 (7)*, 1-17.

Mohamad Nor, N., Lau, L.C., Lee, K.T., Mohamed, A.R., 2013. "Synthesis of activated carbon from lignocellulosic biomass and its applications in air pollution control - a review." *J. Environ. Chem. Eng. 1 (4)*, 658–666.

Nayak, A., Bhushan, B., Gupta, V., Sharma, P., 2017. "Chemically activated carbon from lignocellulosic wastes for heavy metal wastewater remediation: Effect of activation conditions." *J. Colloid Interface Sci.* 493, 228–240.

Neme, I., Gonfa, G., Masi, C., 2022. "Activated carbon from biomass precursors using phosphoric acid: A review." *Heliyon 8*, e11940.

Ngueabouo, A.M.S., Tagne, R.F.T., Tchuifon, D.R.T., Fotsop, C.G., Tamo, A.K., Anagho, S.G., 2022. "Strategy for optimizing the

synthesis and characterization of activated carbons obtained by chemical activation of coffee husk." *Mater. Adv.* 3, 8361–8374.

Oginni, O., Singh, K., Oporto, G., Dawson-Andoh, B., McDonald, L., Sabolsky, E., 2019. "Effect of one-step and two-step H_3PO_4 activation on activated carbon characteristics." *Bioresour. Technol. Rep. 8*, 100307.

Oliveira, L.S., Franca, A.S., Alves, T.M., Rocha, S.D.F., 2008. "Evaluation of untreated coffee husks as potential biosorbents for treatment of dye contaminated waters." *J. Hazard. Mater.* 155, 507–512.

Quyen, V.T., Pham, T.-H., Kim, J., Thanh, D.M., Thang, P.Q., Van Le, Q., Jung, S.H., Kim, T., 2021. "Biosorbent derived from coffee husk for efficient removal of toxic heavy metals from wastewater." *Chemosphere 284*, 131312.

Rahim, A.A., Garba, Z.N., 2016. "Optimization of preparation conditions for activated carbon from *Prosopis africana* seed hulls using response surface methodology." *Desalination Water Treat. 57*, 17985–17994.

Reddy, K.S.K., Al Shoaibi, A., Srinivasakannan, C., 2012. "Activated carbon from date palm seed: process optimization using response surface methodology." *Waste Biomass Valorization 3*, 149–156.

Salleh, N.H.M., Arbain, D., Daud, M.Z.M., Zainalabidin, N., 2014. "Preparation and characterisation of rice husk activated carbon for neutral protease adsorption." *Mater. Res. Innov. 18*, S6-307.

Thuy Luong Thi, T., Ta, H.S., Le Van, K., 2021. "Activated carbons from coffee husk: Preparation, characterization, and reactive red 195 adsorption." *J. Chem. Res. 45*, 380–394.

Wang, J., Liu, H., Yang, S., Zhang, J., Zhang, C., Wu, H., 2014. "Physicochemical characteristics and sorption capacities of heavy metal ions of activated carbons derived by activation with different alkyl phosphate triesters." *Appl. Surf. Sci. 316*, 443–450.

Xu, Z., Lǔ, B., Wu, J., Zhou, L., Lan, Y., 2013. "Reduction of Cr(VI) facilitated by biogenetic jarosite and analysis of its influencing factors with response surface methodology." *Mater. Sci. Eng. C 33*, 3723–3729.

Zhang, Z., Liu, X., Li, D., Gao, T., Lei, Y., Wu, B., Zhao, J., Wang, Y., Wei, L., 2018." Effects of the ultrasound-assisted H_3PO_4 impregnation of sawdust on the properties of activated carbons produced from it." *New Carbon Mater. 33*, 409–416.